# Glass Hardness Modification by Means of Ion Implantation: Electronic Doping versus Surface Composition Effect

*Julien Idé, David Cornil, Amory Jacques, Benjamine Navet, Pierre Boulanger, Lionel Ventelon, Roberto Lazzaroni, David Beljonne, and Jérôme Cornil**

**Critical load measurements point to an improvement in the hardness of a soda–lime glass upon nitrogen implantation. In order to determine whether this improvement originates from electronic doping or surface composition changes induced by ion implantation, a theoretical approach using quantum-chemical and force-field methods combined with X-ray photoelectron spectroscopy is performed. The results indicate that neither an electronic effect nor a lattice distortion appear to be the primary cause of the hardness improvement. It is rather a change in the surface composition leading to a more densely cross-linked and stiffer silica network at the top surface of the glass which is at the origin of this improvement.**

## 1. Introduction

Ion implantation has been widely used in industrial processes since the beginning of the 1970s to dope semiconductors for microelectronics applications, and later for surface treatment of materials such as metals[1,2] and polymers.[3–5] More recently, it has been applied to glasses to improve their optical and mechanical properties,[6–12] although the microscopic origin of these improvements is still unclear. Wang et al.[11] suggested that the surface hardening of a nitrogen-implanted soda–lime glass can be due to the formation of nitrogen–oxygen–silicon complexes. Their formation was evidenced by X-ray photoelectron spectroscopy, (XPS) but no clear evidence of their correlation with surface hardening was provided. On the other hand, surface sodium depletion, due to sputtering (nuclear stopping) or ion migration (electronic stopping), has been also investigated,[10,12,13] though no clear explanation of the relationship between this depletion and surface hardening was proposed. This work stems from the observation that the hardness of a soda–lime glass estimated by AGC by measuring the critical load (technical details are provided in Supporting Information) increases by about 9% (from 7.90 to 8.59 N) upon implantation. A better resistance to scratch has also been noticed. Although the introduction of a significant amount of nitrogen into a glass is known to affect its mechanical properties by creating significant lattice distortions,[14] this cannot be readily expected here when considering the very low amount of nitrogen introduced by implantation (<0.5 at.%). Other different processes triggered by the ion implantation might be at the origin of this improvement of the mechanical properties. On one hand, the nitrogen atoms introduced into the silica network, either in an interstitial or substitutional way, are expected to reshuffle the electronic density distribution within the system and potentially change its hardness; this is referred here to as a doping effect. On the other hand, the implanted ions can collide with the atoms at the surface of the sample and eject or push them deeper into the bulk (i.e., micro-hammering), thus changing the surface composition and most likely the mechanical properties; this is referred here to as surface composition effect. In this context, we investigate through modeling whether doping and/or surface composition effects induced by nitrogen implantation can modify the hardness of glass substrates. Since the hardness measured experimentally by critical load measurements cannot be easily approached at the theoretical level, we focus here on the directly accessible Vickers hardness and determine whether this parameter is likely to be affected by ion implantation. For this purpose, we use a joint theoretical approach in which quantum-chemical methods are used to model the structural and electronic changes upon doping, whereas the influence of the surface composition is studied at the force-field molecular dynamics (MD) level. XPS measurements have been performed on soda–lime glass samples in order to use experimental surface compositions as input for our MD simulations.

Dr. J. Idé, Dr. D. Cornil, Prof. R. Lazzaroni, Prof. D. Beljonne, Prof. J. Cornil
Laboratory for Chemistry of Novel Materials
University of Mons
Place du Parc 20, 7000 Mons, Belgium
E-mail: Jerome.Cornil@umons.ac.be

Dr. A. Jacques, Dr. B. Navet, Dr. P. Boulanger, Dr. L. Ventelon
AGC Technovation Center
Rue Louis Blériot 12, 6041 Charleroi, Belgium

The ORCID identification number(s) for the author(s) of this article can be found under https://doi.org/10.1002/adts.201900039

**DOI: 10.1002/adts.201900039**

## 2. Methodology

### 2.1. Mechanical Properties

Probing the mechanical properties implies assessing the response of the material to an applied load. For most materials, especially for crystals, this response is anisotropic due to a specific structural orientation at the microscopic scale. The only mechanical parameters accounting for this anisotropy are the fourth-order stiffness (C) and compliance ($S = C^{-1}$) tensors directly involved

 © 2019 WILEY-VCH Verlag GmbH & Co. KGaA, Weinheim

in the Hooke's law ($\sigma = C\varepsilon$), which stipulates that for small distortions, the stress ($\sigma$) of a material is proportional to the applied strain ($\varepsilon$).[15] For anisotropic materials, the stiffness tensor is usually measured by resonance-ultrasound spectroscopy, while for isotropic materials it is more common to directly measure the Young's (E), bulk (B), or shear (G) moduli by fitting stress–strain curves. It should also be noted that there is often significant variability in the values obtained when measuring those mechanical properties. The hardness corresponds to the resistance of a material to a localized deformation such as indentation, scratching, cutting, or bending. The lack of a fundamental definition indicates that the hardness is not a basic property of a material, but rather a composite one with contributions from multiple factors. In this spirit, Chen et al. proposed in 2011[16] an empirical expression relating the Vickers hardness of a material to its bulk and shear moduli. In order to make the connection between the elastic behavior of an isotropic aggregate (polycrystalline material) and a single crystal, Voigt and Reuss, respectively, proposed an averaging of stiffness and compliance constants leading to an upper and lower limit of the bulk and shear moduli. Later, Hill has averaged the previous two limit cases to obtain more reasonable values.[17] In this work, the full stiffness and compliance tensors have been calculated by fitting stress–strain curves for both tensile and shear strains. To deal with the non-orthorhombic cells, the strains have been applied in the Cartesian frame, respectively, along the *x*-, *y*-, *z*-axis and in the *xy*-, *yz*-, *zx*-plane. The bulk and shear moduli have then been calculated using Hill's expression in order to access the Vickers hardness via Chen empirical expression, as already used with oxides.[16,18–20] More details on the calculation of the mechanical properties can be found in Supporting Information.

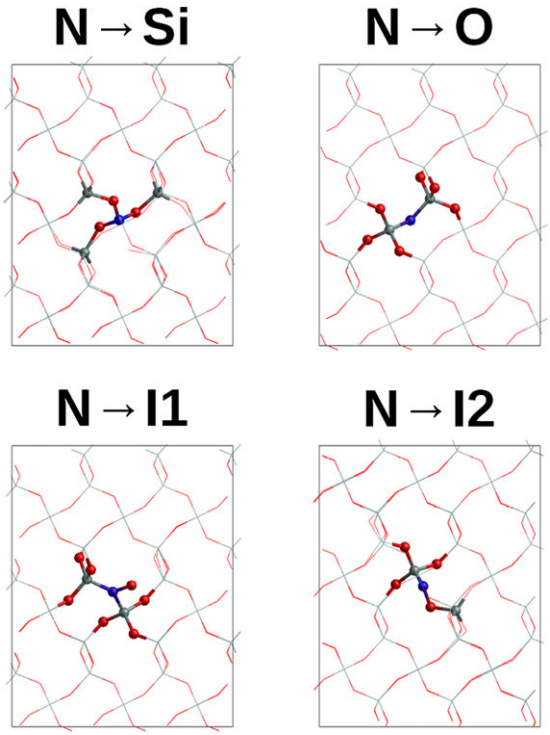


**Figure 1.** Optimized structure of the $\alpha$-quartz doped by substitution (N → Si, N → O) and insertion (N → I1, N → I2). The nitrogen and its first and second neighbors are highlighted. (Si: grey; O: red; N: blue).

### 2.2. Modeling the Doping Effect

The influence of doping has been investigated at the density functional theory (DFT) level using 3D periodic boundary conditions and pseudo-orbitals, as implemented in the SIESTA code.[21] A split-valence double-$\zeta$ basis set augmented by polarization functions have been used, along with standard norm-conservative pseudo-potentials. For the exchange-correlation potential, the generalized gradient approximation using the PBE functional is adopted. For geometry optimizations, the Γ-point approximation has been adopted. For the calculation of electronic properties such as atomic charges, a 3 × 3 × 3 Monkhorst-Pack grid was used. A meshcutoff of 350 Ry was used to resolve the real-space. For each structure, the positions of the atoms were relaxed until all the force components were smaller than 0.01 eV Å$^{-1}$. Lattice parameters have then been optimized until the components of the stress tensor were lower than 0.01 GPa.

Glass has a mixed covalent ($SiO_2$ network) and ionic (cations) character. Since soda–lime glasses are typically made of at least 70% of a covalent $SiO_2$ network, the role of electronic doping has been assessed on pure silica-based model systems in both the crystalline ($\alpha$-quartz) and amorphous (a-$SiO_2$) state in which the impact of the doping of the silicon network should be maximized. It is emphasized that the calculations are performed on neutral systems since the positive charges provided by the ions are expected to be quickly compensated by electrons coming from the outside world in actual experimental conditions. The size of the unit cell was chosen in order to reproduce the experimental nitrogen concentration upon implantation. For a dose of $10^{16}$ ions per square centimeter and a voltage of 35 keV, nitrogen atoms are detected down to 300 nm in depth (see SIMS profile in Supporting Information). By assuming a homogeneous dispersion of the nitrogen atoms inside the material, simulation cells of about 3000 Å$^3$ containing a single nitrogen atom must be adopted to account for the experimental density of implanted atoms. For $\alpha$-quartz, a 3 × 3 × 3 supercell (243 atoms) was generated from the unit cell extracted from the low-temperature X-ray structure (see **Figure 1**.[22] Note that the nitrogen concentration in the implanted systems is so low that the probability for clustering of the dopants is expected to be weak and hence is neglected here. For a-$SiO_2$, a cubic cell (containing the same number of atoms as the $\alpha$-quartz supercell) was generated by annealing a randomly-distributed $SiO_2$ sample using molecular dynamics simulations (see details in Supporting Information). The two kinds of non-implanted cells were then optimized at the DFT level. Since any type of defect is likely to be generated owing to the large amount of energy available upon implantation, several substitutional and interstitial defects have been considered. In the case of substitutional doping, two different simulation cells were prepared by substituting either a silicon (N→Si) or an oxygen atom of the network (N→O) by a nitrogen atom. In the case of interstitial doping, stable positions for the nitrogen atom were searched inside the cavities defined at the intersection of the channels visible along the a-, b- (equivalent by symmetry), and c- directions of the


© 2019 WILEY-VCH Verlag GmbH & Co. KGaA, Weinheim

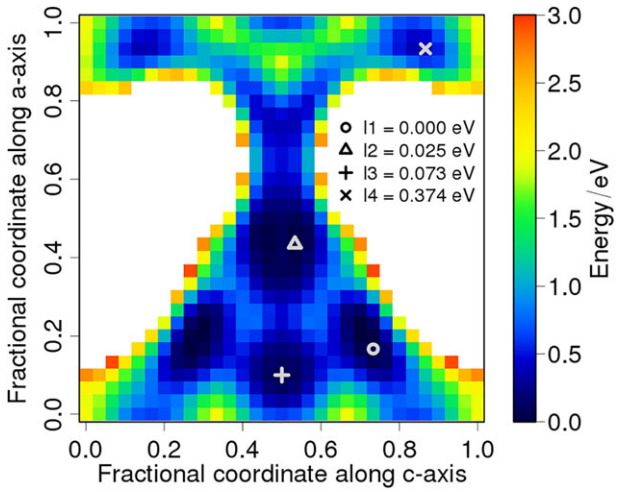


**Figure 2.** Map of the stability of interstitial positions in the ac plane of the $\alpha$-quartz crystal structure. The energy values correspond to the relative stability of the four local minima for an interstitial nitrogen atom.

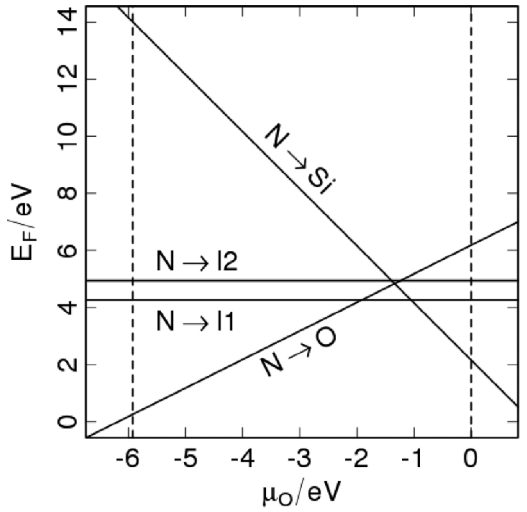


**Figure 3.** Formation energies of substitutional and interstitial defects in nitrogen-doped $\alpha$-quartz. The dashed vertical lines indicate the available range for $\mu_O$.

crystal structure. The preferential interstitial positions have been located in the ac-plane of the $\alpha$-quartz unit cell by computing a potential energy surface using a nitrogen atom as a probe (see **Figure 2**). The lowest two minima displayed in Figure 2 (N→I1 and N→I2) have been selected. For a-$SiO_2$, a nitrogen atom was positioned in the middle of a large empty space of the silica network (N→I). In each case, the cell was fully optimized and its mechanical properties calculated at the DFT level (see Supporting Information for more details).

### 2.3. Modeling the Surface Composition Effect

The influence of the surface composition on the mechanical properties was investigated by means of classical force-field calculations, in analogy with previously reported theoretical studies.[23,24] Here, large simulation cells of soda–lime glass reproducing the experimental compositions have been considered. The concentration profiles of soda–lime glass samples before and after implantation have been measured by XPS and used as input for the calculations probing the evolution of the Vickers hardness with surface composition (i.e., hardness depth profiles).

## 3. Doping Effect

In the case of substitutional doping, the nitrogen atom tends to stay at the position of the substituted atom and, thus, only slightly distorts the network (see Figure 1). In contrast, interstitial nitrogen atoms tend to locally distort the silica network to take the position of an oxygen atom (N→I1) or intercalate between an oxygen and a silicon atom (N→I2). Note that similar defects are observed for amorphous and crystalline silica (see Supporting Information for the amorphous system). In order to evaluate the relative stability of these defects, their formation energies were calculated according to the following equation:

$$E_F = E_{tot}^{X} - \left(E_{tot}^{SiO2} - \mu_X + \mu_N\right) \quad (1)$$

where $E_{tot}^{X}$ and $E_{tot}^{SiO2}$ correspond to the total energies of the implanted and non-implanted systems, respectively, and $\mu_N$ is the chemical potential of a nitrogen atom ($\mu_N = \mu_{N2}/2$). In the case of substitutions, the chemical potential of the substituted species is also involved in the expression ($\mu_X = \mu_{Si}$ or $\mu_O$); otherwise, it is assumed to be zero for insertions. Two different growth conditions were considered to plot the formation energy diagram reported in **Figure 3**, taking either $\mu_O = \mu_{O2}/2 = 0$ (O-rich) or $\mu_{Si} = \mu_{Si}^{diamond}$ (Si-rich) as extreme values. In the last case, $\mu_{Si}$ and $\mu_O$ were related to one another via $\mu_{SiO2} = \mu_{Si} + 2\mu_O$, leading to a $\mu_O$ value of −5.93 eV. In both crystalline and amorphous silica, the N → O defect is the most stable over a large range of $\mu_O$. Close to the O-rich limit ($\mu_O = 0$), the N → Si defect becomes the most stable. Interstitial defects are less stable, especially in amorphous silica in which substitutional defects are always more stable (see Supporting Information). When considering the large amount of energy provided by ion implantation, all these defects are likely to be generated.

The Vickers hardness of each simulation cell has been estimated from its bulk and shear moduli, as described in Supporting Information. The calculated data represented in **Figure 4**, along with the corresponding experimental values for the pristine systems (bulk shear and Young's moduli have been reported in Supporting Information). Since our calculations tend to overestimate the stiffness constants compared to experimental data, the bulk modulus is also over estimated, and in turn the Vickers hardness is under estimated; this has no major implications for our study focusing on relative changes upon implantation. As expected and corroborated by experiment, the calculations indicate that the $\alpha$-quartz is harder than a-$SiO_2$, mainly because of a large difference in the shear modulus. Similarly, crystalline silica always displays a smaller hardness upon doping, mainly due to the decrease in the shear modulus. The hardness variation follows the evolution of the root-mean-square deviation (see Table S3, Supporting Information), indicating that it is sensitive to the


© 2019 WILEY-VCH Verlag GmbH & Co. KGaA, Weinheim

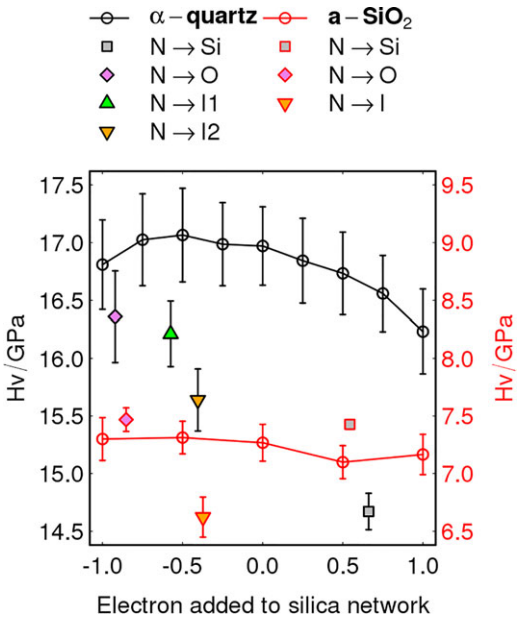


**Figure 4.** Evolution of the Vickers hardness of crystalline (black) and amorphous (red) silica with the virtual doping (lines and empty circles). The Vickers hardnesses obtained by real doping are also reported (filled symbols) for comparison.

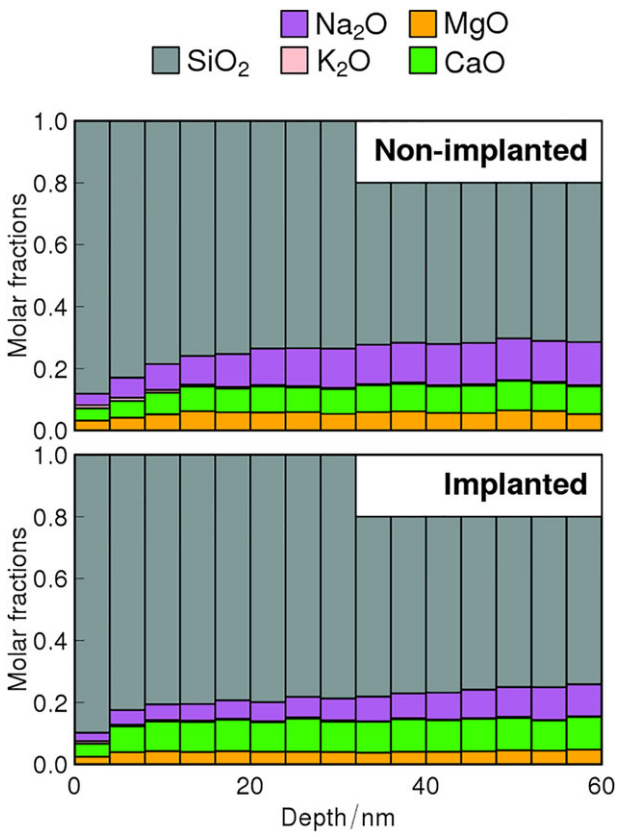


**Figure 5.** Surface composition (molar fraction of oxides) of non-implanted (top) and implanted (bottom) soda–lime glasses.

local distortion of the silica network induced by the formation of the structural defects. For a-$SiO_2$, this correlation is not observed because the degree of distortion is negligible due to the strong degree of amorphization of the system. In order to further disentangle the role of structural amorphization versus charge transfer processes associated to the doping, both pure crystalline and amorphous cells have been virtually doped using the virtual crystal approximation implemented in the SIESTA package.[21] Our simplified procedure consists in removing (adding) a given charge in the network by removing (adding) a corresponding fractional positive (negative) charge on each oxygen atom and in optimizing the unit cell with this modified occupancy. The evolution of the hardness with the virtual doping has been reported in Figure 4. Those calculations demonstrate that such an electronic doping process does not change the hardness of the network, except for slight changes in the crystalline phase associated with minor distortions correlated to the virtual doping process. At this stage, we can thus conclude that the structural and electronic changes associated with the nitrogen implantation have an impact on the mechanical properties in crystalline materials but weakly perturbs them in amorphous silica and by extension in soda–lime glasses in which the robustness of the network is even more lowered by the introduction of ions (Na, K, Ca, Mg) unable to form four chemical bonds with oxygen (i.e., network modifiers).

## 4. Surface Composition

Since it is well established that the hardness can be modified by the surface composition,[25,26] the role of this section is to quantify this effect from the actual experimental compositions. To do so, the surface composition of non-implanted and implanted (dose: $10^{16}$ ions per square centimeter, voltage: 35 keV) soda–lime glasses was analyzed by XPS (see **Figure 5**; experimental details are provided in Supporting Information). As expected, silica (grey bins in Figure 5) is the major component and the other oxides appear in smaller amounts ($Na_2O$: violet; $K_2O$: pink; CaO: green; and MgO: orange).These network modifiers are usually introduced in order to lower the glass transition (≈1475 K for pure $SiO_2$[27]) and hence reduce the production cost. Before implantation, the glass already displays a surface depletion of network modifiers leading to a $SiO_2$-rich region at the top surface of the sample. This depletion is enhanced by nitrogen implantation, as evidenced by the percentage of network modifiers in the 15–45 nm range which drops from ≈27% to ≈21% upon implantation. In our implantation conditions, the glass composition is affected down to 60 nm, where the concentration profiles of the two glasses converge toward the same bulk composition.

The concentration profiles have been divided into 4-nm thick layers for which amorphous simulation cells reproducing their experimental compositions have been prepared. The preparation of our amorphous cells was carried out with MM/MD simulations using the LAMMPS[28] package and the force-field for binary oxides developed by Mc Cormack et al.[29] Each cell was generated as follows: First, atoms were randomly dispersed inside a 4-nm size cubic box (i.e., the same size as the domains


© 2019 WILEY-VCH Verlag GmbH & Co. KGaA, Weinheim

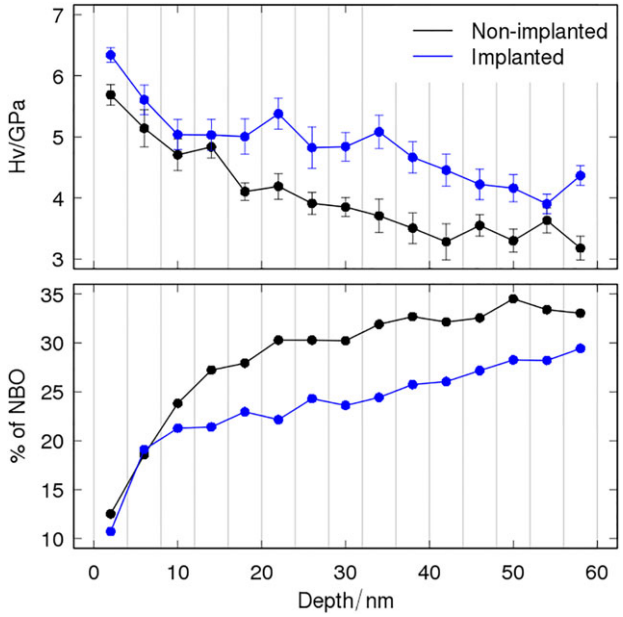


**Figure 6.** Evolution with the surface composition of the Vickers hardness (top) and percentage of non-bridging oxygens (bottom) in the non-implanted (black) and implanted (blue) soda–lime glasses.

within which the experimental compositions were averaged). The number of atoms was chosen in order to respect a given experimental composition and to obtain a starting density of 2.2 g $cm^{-3}$ (experimental density of amorphous silica at room temperature). After minimization, an NVT simulation was performed. The sample was heated to 6000 K to obtain a liquid and then cooled (10 K $ps^{-1}$) down to 300 K to generate an amorphous glass. Finally, the density of the glass was equilibrated for 200 ps at 300 K by running an isotropic NPT simulation. For each experimental composition, the previous procedure was repeated ten times to produce different amorphous models matching the same composition. More details about the validation of the generated amorphous structures are provided in Supporting Information. The evolution of the hardness with the composition was then assessed by calculating the hardness in each layer, before and after implantation. The corresponding hardness profiles are shown in **Figure 6**, top. The degree of polymerization of the silica network was also followed by calculating the percentage of non-bridging oxygens (NBO), that is, oxygen atoms not bonded to two silicon atoms, within each simulation cell (Figure 6, bottom). It is worth noticing that without any treatment, the soda–lime glass is already harder at the surface; this is correlated to the surface depletion in network modifiers favoring the silica network polymerization and hence increasing the hardness. By amplifying the surface depletion of network modifiers, the implantation leads to a further increase in the hardness by about 1 GPa in the 15–45 nm range. Consistently, the NBO abundance is systematically lower in the implanted material, reflecting a more densely cross-linked and stiffer silica network.

The composition effect was further investigated on theoretical models of binary mixtures made of silica and $Na_2O$, $K_2O$, CaO, MgO, or $Al_2O_3$ in order to assess the influence of the different oxides forming a glass on its stiffness. The molar fraction of silica

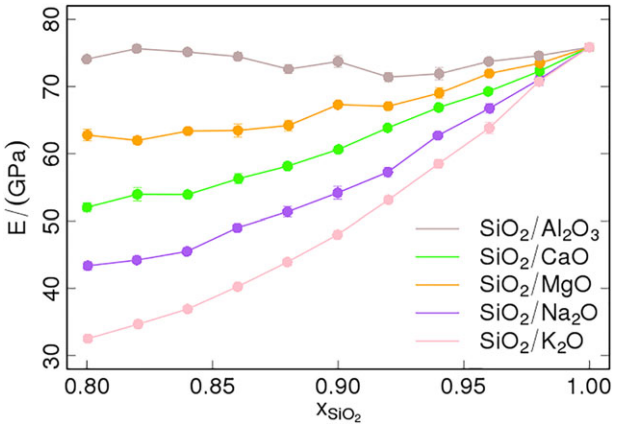


**Figure 7.** Evolution of the Young's modulus of binary mixtures with the $SiO_2$ molar fraction.

was varied from 0.8 to 1.0, and for each composition, the mechanical properties of the mixture were calculated. In order to reduce the computational effort, the shear strains were not considered, allowing thus access to the stiffness (Young's modulus) but not to the Vickers hardness. The stiffness profiles of the model binary mixtures are reported in **Figure 7**. Adding network modifiers ($Na_2O$, $K_2O$, CaO, or MgO) to silica rapidly decreases the stiffness of the mixture, while it is maintained when adding $Al_2O_3$. This behavior is not surprising, since $Al_2O_3$ is known to be an intermediate oxide contributing to the formation of the covalent network of glasses. The impact of $K_2O$ and $Na_2O$ are the most detrimental in terms of stiffness. Since ion implantation mainly reduces the surface concentration of $Na_2O$ in our glasses and the stiffness is reduced by its presence, it is consistent to observe a significant increase in the mechanical properties at the surface of our glass upon ion implantation.

## 5. Conclusions

Since the 1990s, it is known that ion implantation can modify surface composition of a glass (sodium migration) and improve its hardness. The lack of a microscopic understanding of the processes leading to this improvement motivated the present study focusing on nitrogen implantation on a soda–lime glass. The impact of the formation of local nitrogen-based defects and electronic doping has been investigated at the DFT level. Our results show that the formation of local structural defects tends to reduce the hardness of the material when starting from a crystalline structure and that this effect is strongly attenuated in amorphized systems such as glasses; similarly, the purely electronic process of doping has no impact on amorphous materials. Accordingly, we quantified next the effect of changes induced in the surface composition by ion implantation, using XPS measurements as input for classical force-field simulations. Our results demonstrate that ion implantation enhances the surface depletion of network modifiers, which is already present in the non-implanted glass, and favors the polymerization of the silica network at the surface of the glass. This improvement in the degree of polymerization of the silica network at the surface


© 2019 WILEY-VCH Verlag GmbH & Co. KGaA, Weinheim

is found to be the primary reason for an increase in the Vickers hardness of the glass and for changes evidenced by critical load measurements.

Although the doping has no significant effect on the hardness of soda-lime glasses, the picture might be different for alumino-silica glasses in which alumina contributes to the formation of the covalent network of the glass. The changes in the surface composition of alumino-silica glasses upon ion implantation are also expected to be different from those in soda-lime glasses considering the different sodium and calcium diffusion mechanisms at high temperature.[30] Assessing the role of the doping and surface composition changes induced by ion implantation on the hardness of alumino-silica glasses will be the focus of future investigations.

## Supporting Information

Supporting Information is available from the Wiley Online Library or from the author.

## Acknowledgements

D.B. and J.C. are FNRS research directors. This work was supported by the BEWARE Academia program jointly funded by Région Wallonne and the European Commission (grant 1410159 EMOTION). The computing resources were provided by the Consortium des Equipements de Calcul Intensif (CECI), with the support of the Belgian National Fund for Scientific Research (FNRS).

## Conflict of Interest

The authors declare no conflict of interest.

## Keywords

density functional theory, force-field calculations, glass, ion implantation, mechanical properties

Received: February 19, 2019
Revised: April 12, 2019
Published online:

[1] G. Dearnaley, *Thin Solid Films* **1983**, *107*, 315.
[2] S. T. Picraux, *Annu. Rev. Mater. Sci.* **1984**, *14*, 335.
[3] M. Wintersgill, *Nucl. Instrum. Meth. B* **1984**, *1*, 595.
[4] L. B. Bridwell, R. Giedd, Y. Wang, S. Mohite, T. Jahnke, I. Brown, C. Bedell, C. Sofield, *Nucl. Instrum. Meth. B* **1991**, *56–57*, 656.
[5] V. Popok, *Rev. Adv. Mater. Sci.*, **2012**, *30*, 1.
[6] G. W. Arnold, *Radiat. Eff.*, **1982**, *65*, 17.
[7] F. Caccavale, *Pramana*, **1998**, *50*, 653.
[8] G. Battaglin, R. D. Maschio, G. D. Mea, G. D. Marchi, V. Gottardi, M. Guglielmi, P. Mazzoldi, A. Paccagnella, *Nucl. Instrum. Meth. B* **1984**, *1*, 253.
[9] H. Karge, R. Mühle, *Nucl. Instrum. Meth. B* **1992**, *65*, 380.
[10] P. Mazzoldi, *Nucl. Instrum. Methods Phys. Res.*, **1983**, *209–210*, 1089.
[11] C. Wang, Y. Tao, S. Wang, *J. Non-Cryst. Solids*, **1982**, *52*, 589.
[12] N. Skelland, P. Townsend, *J. Non-Cryst. Solids*, **1995**, *188*, 243.
[13] G. Battaglin, G. Mea, G. D. Marchi, P. Mazzoldi, A. Miotello, *Nucl. Instrum. Meth. B* **1984**, *1*, 511.
[14] T. Rouxel, N. Dely, J.-C. Sangleboeuf, S. Deriano, M. LeFloch, B. Beuneu, S. Hampshire, *J. Am. Ceram. Soc.* **2005**, *88*, 889.
[15] P. Vannucci, *General Anisotropic Elasticity*, Springer, Singapore **2018**.
[16] X.-Q. Chen, H. Niu, D. Li, Y. Li, *Intermetallics*, **2011**, *19*, 1275.
[17] R. Hill, *Proc. Phys. Soc. London, Sect. A*, **1952**, *65*, 349.
[18] Q. Chen, F. Cao, T. Csanádi, J. Xu, M. Fu, M. Wang, J. Dusza, *J. Am. Ceram. Soc.* **2018**, *101*, 5138.
[19] E. Kulik, N. Nishiyama, Y. Higo, N. A. Gaida, T. Katsura, *J. Am. Ceram. Soc.* **2019**, *102*, 2251.
[20] R. Belghit, H. Belkhir, D. Heciri, M. Bououdina, M. Kadri, R. Ahuja, *Chem. Phys. Lett.* **2018**, *706*, 684.
[21] J. M. Soler, E. Artacho, J. D. Gale, A. García, J. Junquera, P. Ordejón, D. Sánchez-Portal, *J. Phys.: Condens. Matter*, **2002**, *14*, 2745.
[22] P. Heyliger, H. Ledbetter, S. Kim, *J. Acoust. Soc. Am.*, **2003**, *114*, 644.
[23] Y. Yu, B. Wang, M. Wang, G. Saud, M. Bauchy, *Int. J. Appl. Glass Sci.*, **2017**, *8*, 276.
[24] S. Sundararaman, W.-Y. Ching, L. Huang, *J. Non-Cryst. Solids*, **2016**, *102*, 445.
[25] M. Barlet, J.-M. Delaye, T. Charpentier, M. Gennisson, D. Bonamy, T. Rouxel, C. Rountree, *J. Non-Cryst. Solids*, **2015**, *417-418*, 66.
[26] E. Kilinc, R. Hand, *J. Non-Cryst. Solids*, **2015**, *429*, 190.
[27] M. L. Ojovan, *J. Exp. Theor. Phys. Lett.*, **2004**, *79*, 632.
[28] S. J. Plimpton, *J. Comput. Phys.* **1995**, *117*, 1.
[29] A. Pedone, G. Malavasi, M. C. Menziani, A. N. Cormack, U. Segre, *J. Phys. Chem. B*, **2006**, *192*, 235.
[30] C. C. Claireaux, M.-H. Chopinet, E. Burov, E. Gouillart, M. Roskosz, M. J. Toplis, *Geochim. Cosmochim. Acta*, **2016**, *192*, 235.

 © 2019 WILEY-VCH Verlag GmbH & Co. KGaA, Weinheim